ACS APPLIED MATERIALS & INTERFACES

www.acsami.org

Research Article

Evaluation of the Volumetric Activity of the Air Electrode in a Zinc–Air Battery Using a Nitrogen and Sulfur Co-doped Metal-free Electrocatalyst

Gyutae Nam,[§] Haeseong Jang,[§] Jaekyung Sung,[§] Sujong Chae, Luke Soule, Bote Zhao, Jaephil Cho,* and Meilin Liu*

Cite This: *ACS Appl. Mater. Interfaces* 2020, 12, 57064–57070

Read Online

ACCESS | Metrics & More | Article Recommendations | Supporting Information

ABSTRACT: While numerous oxygen electrocatalysts have been reported to enhance zinc–air battery (ZAB) performance, highly efficient electrocatalysts for the oxygen electrocatalysis need to be developed for broader commercialization of ZABs. Furthermore, areal (instead of volumetric) power density has been used to benchmark the performance of ZABs, often causing ambiguities or confusions. Here, we propose a methodology for evaluating the performance of a ZAB using the volumetric (rather than the areal) power density by taking into consideration the air electrode thickness. A nitrogen and sulfur co-doped metal-free oxygen reduction electrocatalyst (N-S-PC) is used as a model catalyst for this new metric. The electrocatalyst exhibited a half-wave potential of 0.88 V, which is similar to that of the Pt/C electrocatalyst (0.89 V) due to the effects of co-doping and a highly mesoporous structure. In addition, the use of volumetric activity allows fair comparison among different types of air electrodes. The N-S-PC-loaded air electrode demonstrated a higher peak power density (5 W cm^{-3}) than the carbon felt or paper electrode in the ZAB test under the same testing conditions.

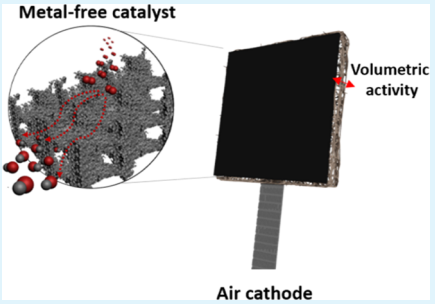

KEYWORDS: *zinc–air batteries, metal-free electrocatalyst, oxygen reduction reaction, volumetric activity, multielemental doping, durability*

1. INTRODUCTION

To fulfill the requirements of energy storage and conversion devices for electric vehicles (EVs) and portable devices, new technology must be developed to achieve high volumetric energy density. Currently, Li-ion batteries (LIBs) are used in these applications as they have inherently high energy and power densities. However, LIBs are notorious for their poor safety, utilization of scarce raw materials, and limited gravimetric energy and power densities for certain applications.[1] Zn–air batteries (ZABs) offer an alternative to LIBs because of their relatively high volumetric energy density (Wh/L), excellent safety, and utilization of abundant raw materials.[2,3] However, ZABs suffer from sluggish oxygen redox kinetics at the air electrode, limiting their widespread adoption.[4] Platinum group metal (PGM) electrocatalysts are commercial catalysts to promote the rate of oxygen reduction reaction (ORR) and reduce the overpotential of the ORR,[5,6] but their scarcity and low stability in alkaline media prohibit their practical use.[5,7] To overcome these issues, significant efforts have been devoted to developing nonprecious metal electrocatalysts with ORR activity, including metal-free electrocatalysts,[4] transition metal alloy electrocatalysts,[8] transition metal–carbon composite electrocatalysts,[9,10] and metal-oxide based electrocatalysts.[11] Among these, the metal-free electrocatalysts have attracted increasing attention due to their low cost. A particularly popular method is the doping of nonmetallic elements such as nitrogen,[12] sulfur,[13] and phosphorous into carbon structures. The dopants are believed to decrease the adsorption energy of oxygen, which facilitates the ORR process.

To characterize the activity of an electrocatalyst for the ORR, the catalyst's half-wave potential (HWP) is measured using a half-cell in a three-electrode (reference, working, and counter electrode) configuration through rotating disk electrode (RDE) measurement. When utilized in a ZAB, performance comparison of different catalysts could be ambiguous due to the use of different air electrodes. Generally, the performance is reported using the areal activity (mA cm^{-2}) of the air electrode. Uncertainties arise using the areal activity due to the varied types of air cathodes with different surface areas and thicknesses resulting in different ORR performances. For example, catalyst-loaded carbon paper and carbon felt are mostly well-known air cathodes for ZABs, while several results

Received: September 18, 2020
Accepted: December 2, 2020
Published: December 14, 2020

https://dx.doi.org/10.1021/acsami.0c16876
ACS Appl. Mater. Interfaces 2020, 12, 57064–57070

have reported ZAB performance with homemade air cathodes.[2,4,8]

Herein, we report a new performance metric by calculating the volumetric activity of a ZAB utilizing a nitrogen and sulfur co-doped carbon electrocatalyst. The metal-free ORR electrocatalyst used in the current work is a polyhedron-shaped nitrogen and sulfur co-doped mesoporous carbon (denoted as N-S-PC) prepared from the heat treatment of zeolitic imidazolate frameworks (ZIFs) and dibenzyl disulfide (DBDS). Thanks to the N and S co-doping effect and mesoporous structure, N-S-PC performed 0.88 V of HWP. In ZAB application, the overpotential and peak volumetric power density (mW cm^{-3}) are reported using three different types of N-S-PC-loaded air electrodes, which are carbon felt, carbon paper, and an in-house air electrode. Among the three different types of air electrodes, the in-house prepared air electrode had the highest peak power density (5000 mW cm^{-3}) and a durable performance at the same discharge volumetric density (20 mA cm^{-3}). The reported volumetric activity representation allows for the direct comparison of ZAB performance regardless of the types of air electrodes and electrocatalysts used. We believe that the volumetric activity metric is a suitable and useful index of commercial success of ZABs and will guide future research direction.

2. EXPERIMENTAL SECTION

2.1. Synthesis of N-S-PC and N-PC electrocatalysts. The N-S-PC catalyst was prepared by simple pyrolyzing of ZIF-8 ($C_8H_{12}N_4Zn$, 99%) and DBDS ($C_{14}H_{14}S_2$, ≥95.0%, Sigma-Aldrich). In detail, 1 g of ZIF-8 and 1 g of DBDS were ground in a mortar for 10 min. The mixed precursor was then heated at 90 °C for 8 h and pyrolyzed in Ar at 1050 °C for 1 h. N-S-PCs at different temperatures were fired in Ar each for 1 h at a heating rate of 5.5 °C min^{-1}. N-PC was prepared by using the same procedures without the DBDS precursor.

2.2. Preparation of the Homemade Air Electrode. The homemade air electrode was prepared by grinding activated carbon (Sigma-Aldrich), a binder (60 wt % PTFE emulsion in water, Sigma-Aldrich), and the as-prepared electrocatalyst at a weight ratio of 67:28:5 for 1 h. Then, the paste was cast onto a Ni foam and calendared to a thickness of 700 μm.

2.3. Fabrication of the Zinc–Air Battery. Fabrication of the zinc–air batteries was made using Zn metal as the anode, a homemade air electrode, carbon paper, and carbon felt as the cathode, and 6 M KOH as the electrolyte. These assembled full cells were tested at a 20 mA cm^{-3} discharge current density. The volume of each cathode is calculated by multiplying the thickness and area of air cathodes.

2.4. Measurement of the Electrochemical Properties. Half-cell rotating disk electrode (RDE) tests were conducted with a glassy carbon electrode (0.196 cm^2 GCE) as a working electrode, Pt wire as a counter electrode, and SCE as a reference electrode (sat. KCl). Before loading the as-prepared electrocatalyst onto the working electrode, glassy carbon, the substrate was polished using alumina paste. The ink composition was 5 mg of catalyst and 50 μL of 5.2 wt % Nafion ionomer solution (Ion Power) and 1.13 mL of ethanol. The ink was sonicated for 20 min. A total of 4.64 μL of ink containing around 19.6 μg of catalyst was loaded onto the working electrode, resulting in a catalyst loading of N-S-PC of 100 μg cm^{-2}. The commercialized Pt/C (20 wt %, HiSPEC 3000, Johnson Matthey) catalyst was prepared as the comparison electrocatalyst by the same process except for using ethanol in the catalyst ink to prevent platinum oxidation. Cyclic voltammetry (CV) experiments were conducted at a 50 mV s^{-1} scan rate in nitrogen- and oxygen-saturated alkaline media. To obtain the Tafel slope, RDE tests with different rpm's were conducted with a 10 mV s^{-1} scan rate (400, 900, 1200, 1600, and 2500 rpm). Current–time (i–t) chronoamperometric responses were measured at 0.5 V vs RHE for 20,000 s. All electrochemical characterization in this work was performed using a bipotentiostat (IviumStat). All electrochemical performances measured with RDE are references vs the reversible hydrogen electrode (RHE).

2.5. Physical and Chemical Characterization. The crystal structure of N-S-PC was analyzed using an XRD (Rigaku Ru-200B) with a Cu Kα (λ= 1.5405 Å) source with a Ni filter and operating at 40 kV and 100 mA. FE-SEM (JEOL 7300) was operated at 10 kV and 20 μA for morphology characterization. HRTEM, elemental mapping, and energy-dispersive spectrum (EDS) analysis were performed with a Tecnai G2 S-Twin at 200 keV. XPS was performed on a MULTILAB 2000 SYSTEM with monochromic Al Kα (E = 1486.6 eV). All binding energies were corrected using the signal, and the C1s peak at 284.5 eV was taken as an internal standard. Raman spectra were obtained using a RENISHAW in a Via Raman microscope with 514 nm Ar^+ laser excitation. The nitrogen adsorption–desorption experiments were performed at 77 K on a Belsorp mini II, BEL JAPAN. Before the BET measurements, samples were degassed at 200 °C for 5 h.

3. RESULTS AND DISCUSSION

Figure 1a schematically depicts the areal (mA cm^{-2}) and volumetric (mA cm^{-3}) activity of a ZAB. Measuring the areal

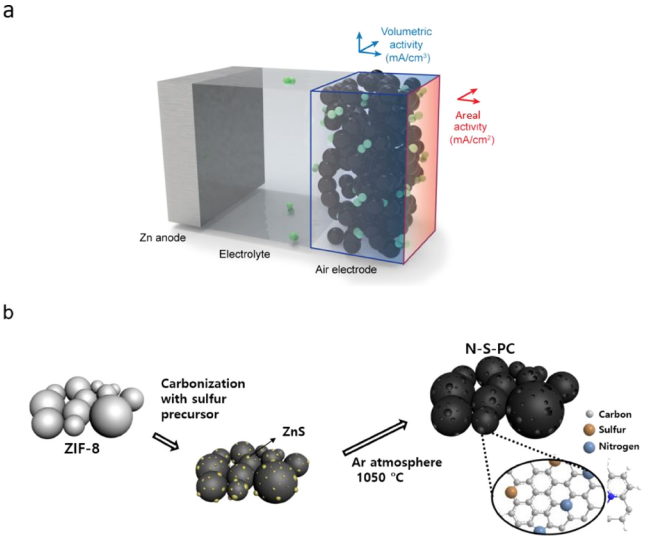

Figure 1. (a) Schematic illustration of areal activity and volumetric activity expression of zinc–air battery; (b) synthesis procedure scheme of N-S PC.

activity of the cell is ambiguous due to the inability to count all active sites of the air electrode. Thus, the volumetric activity expression may be useful for ZAB performance comparison between different types of air electrodes because the gas diffusion layer in air cathodes contributes to the performance, making the measurement of electrocatalyst activity alone difficult. Volumetric activity forgoes the measurement of active sites and only expresses performance in terms of the applied current.

Figure 1b shows a schematic of the metal-free electrocatalyst synthesis procedure (nitrogen and sulfur co-doped porous carbon denoted as N-S-PC). Mixtures of ZIF-8 and DBDS (N-S-PC precursors) were pyrolyzed in Ar at 1050 °C with a heating rate of 5.5 °C min^{-1}, while ZIF-8 was used as the N precursor and DBDS was used as the S precursor. The annealing temperature was 1050 °C because the crystallinity of the carbon sample derived from this temperature is the highest, as can be seen in Figure S1. After heating, the porous N and S

https://dx.doi.org/10.1021/acsami.0c16876
ACS Appl. Mater. Interfaces 2020, 12, 57064–57070

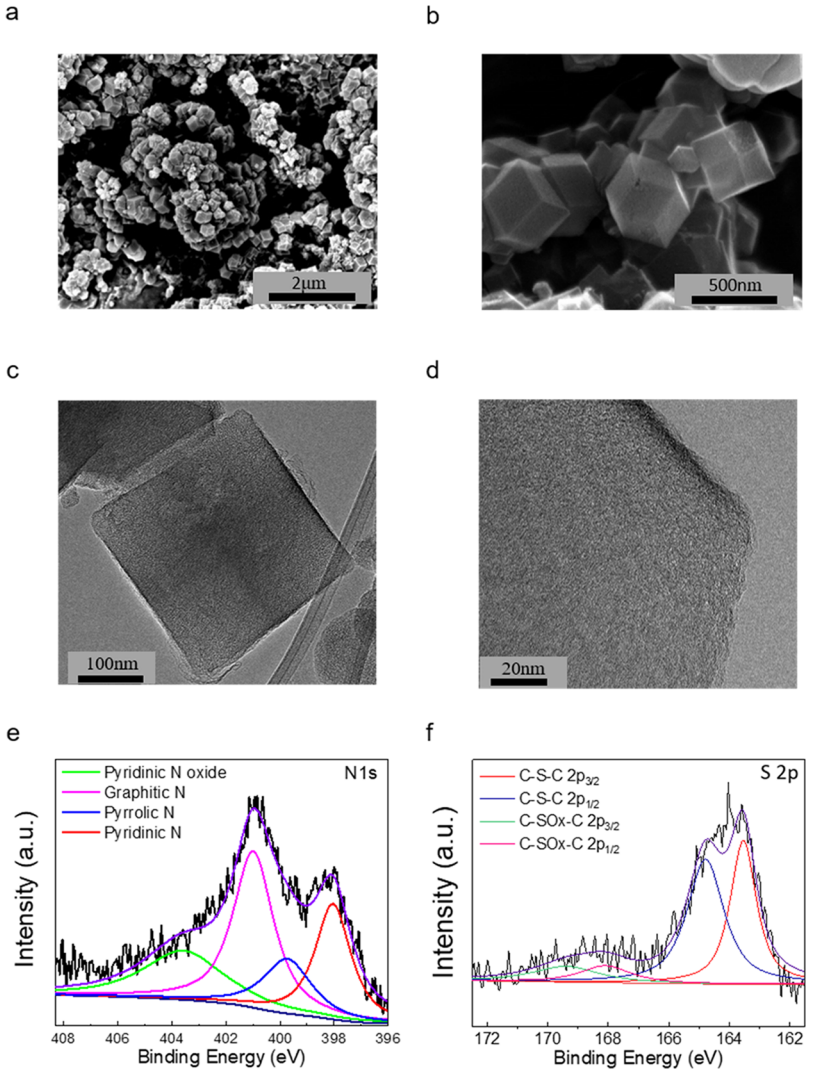

Figure 2. (a) Low-magnification SEM image of N-S-PC, (b) polyhedron morphology observed via high-magnification SEM image of N-S-PC, (c, d) TEM images, (e, f) XPS spectra of (e) N1s and (f) S2p of the N-S-PC sample.

co-doped carbon product is obtained after evaporation of Zn. Moreover, we have also prepared a N-doped porous carbon (N-PC) electrocatalyst for comparison. The detailed synthetic procedures of the as-prepared electrocatalysts are explained in the Experimental Section.

The structure of N-S-PC was analyzed using SEM, TEM, XPS, and XRD analysis. As shown in Figure 2a–d, a polyhedron morphology was observed under SEM and TEM. Through scanning transmission electron microscopy–energy-dispersive X-ray spectroscopy (STEM–EDS) mapping, we observed that N and S are incorporated into the porous carbon structure (Figure S2). No Zn from ZIF-8 has been found in N-S-PC as Zn has a boiling point of 908 °C and likely evaporated during pyrolysis.[14] To characterize the chemical bonding information of N-S-PC, XPS analysis was performed. The survey scan of N-S-PC shows the C1s peak (~284.5 eV), O1s peak (~531.5 eV), N1s peak (401.0 eV), and two S peaks (~164.5 0 eV, ~227.5 eV), which indicates the presence of elemental N (4.56 at %) and S (1.12 at %) in N-S-PC (Figure 2e,f and Figure S3). To confirm that S and N were doped into the structure, elemental scans were performed. As shown in Figure 2e, pyridinic N (~398.1 eV), pyrrolic N (~399.8 eV), graphitic N (401.0 eV), and pyridine oxide (403.8 eV) peaks were observed, indicating the successful N doping into carbon. N-PC also exhibits the same peak position except for S peaks (Figure S3). It has been reported that graphitic N is a more favorable active site for the ORR than pyridinic N; however, in the case of the other N species, pyrrolic N or oxidized N had a negligible effect on the electrocatalytic activity of N-doped carbon materials.[15,16] The XPS profiles of the S2p spectrum of N-S-PC are shown in Figure 2f. The first two peaks are C–S–C $2p_{3/2}$ (163.7 eV) and C–S–C $2p_{1/2}$ (~164.9 eV), which are known as effective active sites for the ORR. The sulfur oxidation peaks assigned to the C–SO_x–C $2p_{3/2}$ (168.0 eV) and C–SO_x–C $2p_{1/2}$ (169.5 eV) are known to be electrochemically inactive for the ORR.[13,17,18] According to Lee et al., however, C-SO_x-C may also participate in the ORR by acting as an adsorption site for oxygen molecules owing to the difference in electron negativity of the graphene layer and C-SO_x-C sites.[19] XRD and Raman analyses were conducted to identify the crystal structure of N-S-PC and N-PC (Figure S4). The XRD patterns of both N-S-PC and N-PC display two broad peaks at 22 and 43°, which are assigned to the characteristic carbon (002) and (100)/(101) diffraction planes, indicating that ZIF-8 was completely converted to the carbon. There are no peaks attributed to zinc metal due to

https://dx.doi.org/10.1021/acsami.0c16876
ACS Appl. Mater. Interfaces 2020, 12, 57064–57070

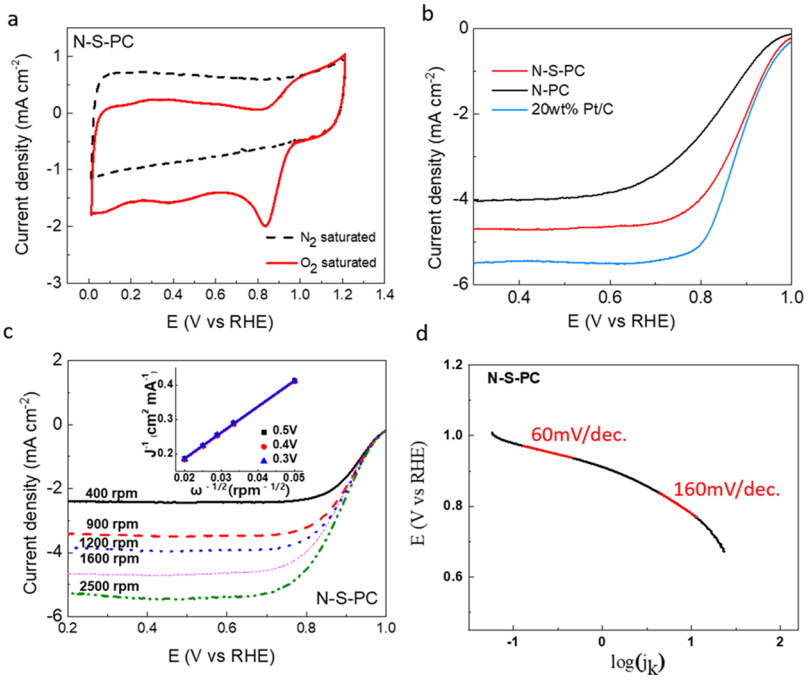

Figure 3. Electrochemical analysis of the (a) cyclic voltammetry of N_2 (black dot)- and O_2 (red solid)-saturated conditions. (b) Oxygen reduction profiles of Pt/C, N-PC, and N-S-PC in rotating disk electrode measurement. (c) Linear sweep voltammetry with different rotating speeds of N-S-PC and Levich equation applied profile (inset). (d) Corresponding Tafel slope of N-S-PC.

its evaporation under pyrolysis.[20] To further quantify the carbon structure, Raman spectroscopy was used. The peak at 1575 cm^{-1} (G peak) indicates the planar motion of the sp^2-hybridized carbon atom, while the peak at 1350 cm^{-1} is the D peak attributed to the breakdown of symmetry of carbon atoms with dangling bonds at the edge of the plane in disordered graphite.[14] The intensity ratio of the peaks within the ordered and disordered sp^2-hybridized carbon gives information about the planar extension of the symmetry of the graphene layer. The intensity ratios of I_D/I_G for N-PC and N-S-PC are about 1.15 and 1.12, respectively, which suggest that ZIF-8 was converted to amorphous carbon (Figure S4). In addition, the TEM images of both N-PC and N-S-PC exhibit a similar morphology (Figure S3c,d). To gain further detailed structural information, we obtained HR-TEM images of N-S-PC. The *d* spacing of graphite (002) is shown in the TEM images along with the amorphous phase indicating the turbostatic carbon structure (Figure S5).

To measure the porosity of N-S-PC, the nitrogen adsorption−desorption isotherms of all samples were measured. The low relative pressure region is related to micropores while high relative pressure region indicates presence of mesopores.[21,22] Most of the nitrogen is adsorbed in the low relative pressure region in the case of ZIF-8 (Figure S6). These results indicate that ZIF-8 consists primarily of micropores. The Barrett, Joyner, and Halenda (BJH) method is used to calculate the pore size distribution. The mesoporous specific surface area of N-S-PC is 634.3 $m^2\ g^{-1}$ (as shown in Table S1).

The electrocatalytic behavior of the N-PC and N-S-PC catalysts was measured by cyclic voltammetry (CV) conducted in a 0.1 M KOH solution saturated with N_2 or O_2. Both N-S-PC and N-PC exhibit a reduction peak in the O_2-saturated solution and no peak in the N_2-saturated solution (Figure 3a and Figure S7). This implies that both N-PC and N-S-PC are active for the ORR. The ORR catalytic activities were measured with RDE equipment. Even though N-S-PC had a lower limiting current density than the Pt/C electrocatalyst, linear sweep voltammograms (LSVs) in Figure 3b indicate that the HWP of N-S-PC is 0.88 V, whereas the HWPs of Pt/C and N-PC are 0.89 V and 0.81 V, respectively. To quantify the ORR kinetics, the Koutechky−Levich (K−L) method was conducted using an RDE at different rotation rates (ω) of 400, 900, 1200, 1600, and 2500 rpm (N-S-PC in Figure 3c). The ORR transfer number can be calculated from the K−L equation.[8,9] In order to obtain the maximum oxidant capacity of O_2, oxygen should be reduced via a four-electron pathway. Figure S8 shows the calculated electron transfer numbers using a linear fit of the K−L plot. The calculated average electron transfer number of N-S-PC is 3.73. These results show that N-S-PC shows a close to four-electron pathway for the ORR similar to that of the Pt/C electrocatalyst (3.84).

To investigate the intrinsic kinetic activity of the as-prepared electrocatalyst, the Tafel plot was measured. The Tafel slope derived from kinetic current density (J_k) gives information about the overall resistance of the ORR process (Figure 3d). In the low overpotential region, which is above 0.8 V, is regarding to surface electrochemistry reaction rate of ORR process. The lower overpotential region Tafel slope of N-S-PC (60 mV dec^{-1}) is the same as that of Pt/C (60 mV dec^{-1}).[23] In the high overpotential region where the ORR depends on a mass transfer reaction, N-S-PC exhibited a higher Tafel slope (160 mV dec^{-1}) than Pt/C (120 mV dec^{-1}), which means a lower kinetic activity of N-S-PC than that of Pt/C at the high overpotential region. The results imply that the rate-determining step of the N-S-PC catalyst is a one-electron transfer reaction due to the material's high intrinsic catalytic ability and improved oxygen diffusion through the mesoporous structure. In addition, chronoamperometric responses were measured to evaluate the durability of N-S-PC and Pt/C. The as-prepared catalysts were held at 0.7 V vs RHE for 20,000 s in

https://dx.doi.org/10.1021/acsami.0c16876
ACS Appl. Mater. Interfaces 2020, 12, 57064−57070

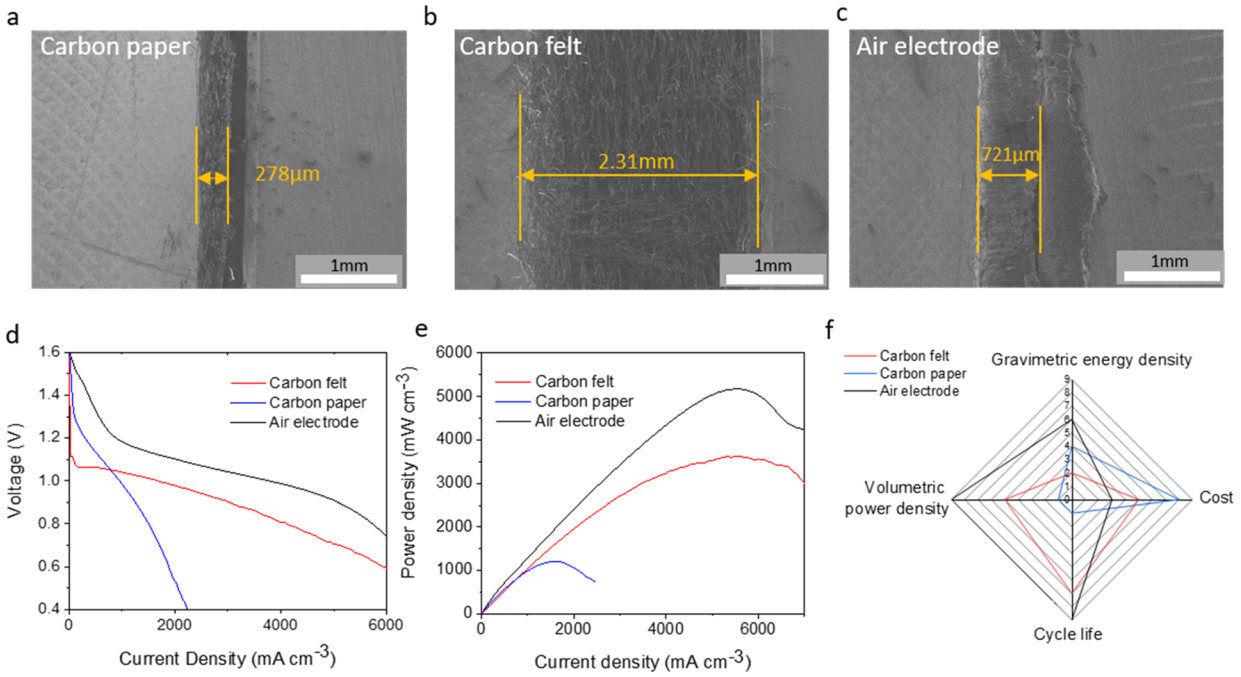

Figure 4. SEM cross-sectional images of air electrodes. (a) Carbon paper, (b) carbon felt, and (c) in-house air electrode. (d) Zn−air battery voltage−current density profiles of N-S-PC loaded air electrodes. (e) Volumetric power density profiles of N-S-PC loaded air electrodes. (f) Spider plot of three different types of air electrode.

O_2-saturated 0.1 M KOH solution at 1600 rpm. As shown in Figure S9a, N-S-PC shows a current retention of 92.2%, while the retention of Pt/C is 87.7%. These results confirm that N-S-PC has improved electrochemical durability compared to commercial Pt/C. Subsequently, the *I*−*t* chronoamperometric responses to methanol were measured for N-S-PC and Pt/C (Figure S9b). When 1 M methanol was added to O_2-saturated 0.1 M KOH, there was no apparent ORR current change at the N-S-PC. On the other hand, the Pt/C ORR activity decreased rapidly, implying that N-S-PC is also usable for a direct-methanol fuel cell by proving the capability for methanol tolerance.

In order to have a fair comparison of the Zn−air battery performance of the N-S-PC and N-PC electrocatalysts, we have prepared N-S-PC and N-PC loaded in-house air electrodes. As shown in Figure S10, N-S-PC and N-PC loaded in-house air electrodes show 722 and 720 μm thickness, respectively. Thus, we have determined volumetric activity by performing ZAB tests. The N-S-PC loaded in-house air electrode had a higher operation voltage and longer lifetime than the N-PC-loaded in-house air electrode at 20 mA cm^{-3} discharge current density.

Comprehensively, there are two reasons why N-S-PC exhibits excellent electrocatalytic performance. The first reason is the increased number of mesopore. These pores facilitate mass transport and smooth diffusion of electrolyte and oxygen during the chemical reaction, so products can be produced quickly. Second, the synergetic effect of N and S dual-doped carbon improves ORR performance. The ORR activity correlates to the charge and spin density of the carbon material. As differences in electronegativity can modulate the charge and spin density of the material, the activity of the material can also be modulated. According to a recent paper by the Qiao group that examined the spin and charge density of graphene, when S and N are simultaneously incorporated into the graphene, their combination exhibits a maximum value. On the other hand, N-doped graphene shows a low spin and charge density. The synergistic effect of co-doped S and N comes from a mixed distribution of spin and charge densities in N-S-PC resulting in good ORR catalytic performance.[12,24]

To evaluate the volumetric activity of a ZAB with a metal-free electrocatalyst, we loaded N-S-PC onto three different types of air electrodes: an in-house air electrode, commercial carbon paper, and carbon felt. The homemade air electrode is prepared using a one-layer method with a mixture of N-S-PC, activated charcoal, and polymeric binder (see the Experimental Section). For the other two air electrodes, we dropped the N-S-PC ink to the carbon paper and carbon felt and dried them in the oven at 60 °C. The thickness of each air electrode was measured using SEM analysis of the cross section (Figure 4a−c). Carbon paper had the smallest thickness, and carbon felt had the largest thickness. The calculated volumes of each air electrode were 0.111, 0.924, and 0.288 cm^3 (carbon paper, carbon felt, and in-house air electrode, respectively). All air electrodes possessed the same amount of N-S-PC electrocatalyst (50 mg in each air electrode).

In order to compare different types of air electrodes using the volumetric activity expression, we performed ZAB tests and used the calculated volumes. To get current density versus voltage plots, a scanning discharge current was applied with a scan rate of 10 mA s^{-1} (Figure 4d). Among the three candidates, the in-house air electrode shows the best performance during the linear current scanning process. The homemade air electrode had a volumetric power density of 5070 mW cm^{-3}, while carbon felt and carbon paper had power densities of 3410 and 1243 mW cm^{-3}, respectively (Figure 4e). At 20 mA cm^{-3} discharge current density, the in-house air electrode showed a longer operation time than both the carbon paper and felt electrodes (Figure S11). In addition, the gravimetric energy density (mAh g^{-1}) of the three air

https://dx.doi.org/10.1021/acsami.0c16876
ACS Appl. Mater. Interfaces 2020, 12, 57064−57070

electrodes was calculated (weight of air electrode is 0.0294, 0.370, and 0.250 g for carbon paper, carbon felt, and in-house air electrode, respectively) to be 770.2, 698.5, and 806.4 mAh g^{-1} (carbon paper, carbon felt, and in-house air electrode, respectively). The performance, cost, and stability of the three air electrodes are depicted in a spider plot shown in Figure 4f.

While many electrocatalysts have been reported for use in ZABs, a lack of a standardized performance guideline makes it challenging to compare their activities. By using a volumetric activity expression for the cathodes, the catalyst's volumetric power density, durability, and gravimetric energy density when used in a ZAB can be used as a fair comparison index.

4. CONCLUSIONS

In summary, we measured the volumetric activity of a metal-free electrocatalyst in a ZAB. It was shown that volumetric capacity is a more reasonable metric of performance for commercial applications. The metal-free electrocatalyst used in the current work was a N and S co-doped mesoporous carbon derived from the pyrolysis of ZIF and DBDS. N-S-PC had a similar HWP to Pt/C and higher HWP than N-PC. The high performance of the as-prepared electrocatalyst was attributed to the enhancement in the charge transfer ability of carbon by the difference of electronegativity of N and S, the numerous active sites, and the facilitated ORR process in the mesoporous framework. Volumetric activity represented by ZAB results proved that the N-S-PC had better operation voltage and stability than N-PC. In addition, three different types of air electrodes were used to evaluate the performance of N-S-PC using volumetric activity and power density. It was shown that even when air electrodes of different thicknesses and porosities were used, the performance of the electrocatalyst was found to be comparable, validating the use of volumetric density as a reasonable performance standard for ZABs.

■ ASSOCIATED CONTENT

Supporting Information

The Supporting Information is available free of charge at https://pubs.acs.org/doi/10.1021/acsami.0c16876.

Table S1: Measured pore values of ZIF-8 and N-S-PC; Figure S1: Raman spectra of heat-treated N-S-PC at 800, 900, 1000, and 1050 °C; Figure S2: STEM−EDS mapping images of N-S-PC; Figure S3: XPS profile of N-S-PC and N-PC and N 1s XPS spectra of N-PC; Figure S4: XRD spectra of N-PC, N-S-PC, and ZIF-8; Raman spectra of N-PC, N-S-PC, and ZIF-8; TEM images of N-PC and N-S-PC; Figure S5: high-magnification HR-TEM images of N-S-PC with graph showing the lattice spacing of the (002) graphite plane; Figure S6: nitrogen adsorption−desorption isotherm of ZIF-8, N-PC, and N-S-PC; Figure S7: cyclic voltammetry of N-PC with a scan rate of 50 mV s^{-1} in O_2- and N_2-saturated 0.1 M KOH solution; Figure S8: calculated electron transfer number (n) of the N-S-PC and Pt/C electrocatalysts; Figure S9: Chronoamperometric response of the N-S-PC and Pt/C electrocatalyst in O_2-saturated 0.1 M KOH; methanol tolerance experiment by adding methanol at 100 s during the chronoamperometric process; Figure S10: SEM cross-sectional images of the N-PC-loaded air electrode and N-S-PC-loaded air electrode; Zn−air battery discharge profiles of the N-S-PC-loaded air electrode and N-PC-loaded air electrode at a 20 mA cm^{-3} discharge current density; Figure S11: zinc−air battery discharge profiles of the N-S-PC electrocatalyst loaded with three different air electrodes (carbon paper, carbon felt, and in-house air electrode) at a 20 mA cm^{-3} discharge current density (PDF)

■ AUTHOR INFORMATION

Corresponding Authors

Jaephil Cho − *Department of Energy Engineering, Department of Energy and Chemical Engineering, Ulsan National Institute of Science and Technology (UNIST), Ulsan 44919, Republic of Korea;* orcid.org/0000-0002-3890-1432; Email: jpcho@unist.ac.kr

Meilin Liu − *School of Materials Science and Engineering, Georgia Institute of Technology, Atlanta, Georgia 30332-0245, United States;* orcid.org/0000-0002-6188-2372; Email: meilin.liu@mse.gatech.edu

Authors

Gyutae Nam − *School of Materials Science and Engineering, Georgia Institute of Technology, Atlanta, Georgia 30332-0245, United States; Department of Energy Engineering, Department of Energy and Chemical Engineering, Ulsan National Institute of Science and Technology (UNIST), Ulsan 44919, Republic of Korea*

Haeseong Jang − *Department of Energy Engineering, Department of Energy and Chemical Engineering, Ulsan National Institute of Science and Technology (UNIST), Ulsan 44919, Republic of Korea*

Jaekyung Sung − *Department of Energy Engineering, Department of Energy and Chemical Engineering, Ulsan National Institute of Science and Technology (UNIST), Ulsan 44919, Republic of Korea*

Sujong Chae − *Department of Energy Engineering, Department of Energy and Chemical Engineering, Ulsan National Institute of Science and Technology (UNIST), Ulsan 44919, Republic of Korea*

Luke Soule − *School of Materials Science and Engineering, Georgia Institute of Technology, Atlanta, Georgia 30332-0245, United States*

Bote Zhao − *School of Materials Science and Engineering, Georgia Institute of Technology, Atlanta, Georgia 30332-0245, United States;* orcid.org/0000-0003-1236-6862

Complete contact information is available at: https://pubs.acs.org/10.1021/acsami.0c16876

Author Contributions

§G.N., H.J., and J.S. contributed equally.

Notes

The authors declare no competing financial interest.

■ ACKNOWLEDGMENTS

This work was supported by the 2019 Research Funds (1.190002.01) of the Ulsan National Institute of Science and Technology (UNIST) and the US National Science Foundation under award number DMR-1742828. The authors acknowledge the financial supports from the Basic Science Research Program through the National Research Foundation of Korea (NRF) funded by the Ministry of Education (NRF-2018R1D1A1B07045504). We thank the Gwangju Institute of Science and Technology (GIST) for the kind help during XRD and Raman measurements.

REFERENCES

(1) Li, M.; Lu, J.; Chen, Z.; Amine, K. 30 Years of Lithium-Ion Batteries. *Adv. Mater.* **2018**, *30*, 1800561.

(2) Li, Y.; Gong, M.; Liang, Y.; Feng, J.; Kim, J. E.; Wang, H.; Hong, G.; Zhang, B.; Dai, H. Advanced zinc-air batteries based on high-performance hybrid electrocatalysts. *Nat. commun.* **2013**, *4*, 1805.

(3) Parker, J. F.; Chervin, C. N.; Pala, I. R.; Machler, M.; Burz, M. F.; Long, J. W.; Rolison, D. R. Rechargeable nickel−3D zinc batteries: An energy-dense, safer alternative to lithium-ion. *Science* **2017**, *356*, 415−418.

(4) Zhang, J.; Zhao, Z.; Xia, Z.; Dai, L. A metal-free bifunctional electrocatalyst for oxygen reduction and oxygen evolution reactions. *Nat. nano.* **2015**, *10*, 444−452.

(5) Wu, G.; More, K. L.; Johnston, C. M.; Zelenay, P. High-performance electrocatalysts for oxygen reduction derived from polyaniline, iron, and cobalt. *Science* **2011**, *332*, 443−447.

(6) Marković, N. M.; Schmidt, T. J.; Stamenković, V.; Ross, P. N. Oxygen Reduction Reaction on Pt and Pt Bimetallic Surfaces: A Selective Review. *Fuel Cells* **2001**, *1*, 105−116.

(7) Shao, M.; Chang, Q.; Dodelet, J. P.; Chenitz, R. Recent Advances in Electrocatalysts for Oxygen Reduction Reaction. *Chem Rev* **2016**, *116*, 3594−3657.

(8) Nam, G.; Son, Y.; Park, S. O.; Jeon, W. C.; Jang, H.; Park, J.; Chae, S.; Yoo, Y.; Ryu, J.; Kim, M. G.; Kwak, S. K.; Cho, J. A Ternary Ni46Co40Fe14 Nanoalloy-Based Oxygen Electrocatalyst for Highly Efficient Rechargeable Zinc−Air Batteries. *Adv. Mater.* **2018**, *30*, 1803372.

(9) Amiinu, I. S.; Liu, X.; Pu, Z.; Li, W.; Li, Q.; Zhang, J.; Tang, H.; Zhang, H.; Mu, S. From 3D ZIF nanocrystals to Co−Nx/C nanorod array electrocatalysts for ORR, OER, and Zn−air batteries. *Adv. Funct. Mater.* **2018**, *28*, 1704638.

(10) Masa, J.; Xia, W.; Muhler, M.; Schuhmann, W. On the Role of Metals in Nitrogen-Doped Carbon Electrocatalysts for Oxygen Reduction. *Angew. Chem. Int. Ed.* **2015**, *54*, 10102−10120.

(11) Suntivich, J.; Gasteiger, H. A.; Yabuuchi, N.; Nakanishi, H.; Goodenough, J. B.; Shao-Horn, Y. Design principles for oxygen-reduction activity on perovskite oxide catalysts for fuel cells and metal−air batteries. *Nat. Chem.* **2011**, *3*, 546−550.

(12) Zheng, Y.; Jiao, Y.; Ge, L.; Jaroniec, M.; Qiao, S. Z. Two-Step Boron and Nitrogen Doping in Graphene for Enhanced Synergistic Catalysis. *Angew. Chem. Int. Ed.* **2013**, *52*, 3110−3116.

(13) Yang, Z.; Yao, Z.; Li, G.; Fang, G.; Nie, H.; Liu, Z.; Zhou, X.; Chen, X. A.; Huang, S. Sulfur-doped graphene as an efficient metal-free cathode catalyst for oxygen reduction. *ACS nano* **2011**, *6*, 205−211.

(14) Tuinstra, F.; Koenig, J. L. Raman Spectrum of Graphite. *The Journal of Chemical Physics* **1970**, *53*, 1126−1130.

(15) Niwa, H.; Horiba, K.; Harada, Y.; Oshima, M.; Ikeda, T.; Terakura, K.; Ozaki, J.-I.; Miyata, S. X-ray absorption analysis of nitrogen contribution to oxygen reduction reaction in carbon alloy cathode catalysts for polymer electrolyte fuel cells. *J. Power Sources* **2009**, *187*, 93−97.

(16) Zheng, B.; Wang, J.; Wang, F.-B.; Xia, X.-H. Synthesis of nitrogen doped graphene with high electrocatalytic activity toward oxygen reduction reaction. *Electrochem. Commun.* **2013**, *28*, 24−26.

(17) Buckel, F.; Effenberger, F.; Yan, C.; Gölzhäuser, A.; Grunze, M. Influence of Aromatic Groups Incorporated in Long-Chain Alkanethiol Self-Assembled Monolayers on Gold. *Adv. Mater.* **2000**, *12*, 901−905.

(18) Choi, C. H.; Park, S. H.; Woo, S. I. Heteroatom doped carbons prepared by the pyrolysis of bio-derived amino acids as highly active catalysts for oxygen electro-reduction reactions. *Green Chem.* **2011**, *13*, 406−412.

(19) Eissa, A. A.; Kim, N. H.; Lee, J. H. Rational Design of Highly Mesoporous Fe−N−C/Fe3C/C−S−C Nanohybrid with Dense Active Sites for Superb Electrocatalysis of Oxygen Reduction. *J. Mater. Chem. A* **2020**, 23436.

(20) Plaza, S.; Mazurkiewicz, B.; Gruziński, R. Thermal decomposition of dibenzyl disulphide and its load-carrying mechanism. *Wear* **1994**, *174*, 209−216.

(21) Sing, K. S. Reporting physisorption data for gas/solid systems with special reference to the determination of surface area and porosity (Recommendations 1984). *Pure and applied chem.* **1985**, *57*, 603−619.

(22) Khalili, N. R.; Campbell, M.; Sandi, G.; Golaś, J. Production of micro-and mesoporous activated carbon from paper mill sludge: I. Effect of zinc chloride activation. *Carbon* **2000**, *38*, 1905−1915.

(23) Ma, L.; Chu, D.; Chen, R. Comparison of ethanol electro-oxidation on Pt/C and Pd/C catalysts in alkaline media. *Int. J. Hydrog. Energy* **2012**, *37*, 11185−11194.

(24) Liang, J.; Jiao, Y.; Jaroniec, M.; Qiao, S. Z. Sulfur and Nitrogen Dual-Doped Mesoporous Graphene Electrocatalyst for Oxygen Reduction with Synergistically Enhanced Performance. *Angew. Chem. Int. Ed.* **2012**, *51*, 11496−11500.

https://dx.doi.org/10.1021/acsami.0c16876
ACS Appl. Mater. Interfaces 2020, 12, 57064−57070